

OPEN

Ferromagnetic excess moments and apparent exchange bias in FeF₂ single crystals

D. C. Joshi*, P. Nordblad & R. Mathieu

The anisotropic antiferromagnet FeF₂ has been extensively used as an antiferromagnetic layer to induce exchange bias effects in ferromagnetic/antiferromagnetic bilayers and heterostructures. In this work, an apparent exchange bias occurring in the low temperature hysteresis loops of FeF₂ single crystals is investigated. A detailed investigation of the hysteresis and remnant magnetization indicates that the observation of an apparent exchange bias in FeF₂ stems from an intrinsic excess moment associated with a distortion of the antiferromagnetic structure of piezomagnetic origin.

The iron fluoride FeF₂ has been extensively used as an antiferromagnetic layer to induce exchange bias effects in ferromagnetic/antiferromagnetic bilayers and heterostructures, a phenomenon of large interest in technological applications such as magnetoresistive read heads and spintronics¹. The strongly anisotropic uniaxial antiferromagnet FeF₂ is an almost ideal realization of a 3d-Ising model system. It exhibits an antiferro- to paramagnetic transition across the Néel temperature $T_N = 78.4\text{ K}$ ². Analyses of the critical behavior of the specific heat, derived from direct measurements² and the derivative of the temperature dependence of the linear birefringence $d(\Delta n)/dT$, yields a critical exponent $\alpha = 0.11$ ³ in agreement with analytic theory⁴. The system is a highly anisotropic material with an anisotropy energy hundred times larger as compared to MnF₂, another family member of 3d-metal fluorides^{5,6}. Internal random stress in such a system may generate a weak spontaneous magnetic moment, piezomagnetic response, due to unbalanced magnetic moments in the two sub-lattices⁷. Previous studies of the temperature dependence of the excess moment shows that it gradually decreases with increasing temperature and approaches zero at T_N ⁸. In the antiferromagnetic state, the spontaneous moment is locked in the cooling field direction and becomes independent of the applied magnetic field and in the transition region, this moment is proportional to the staggered magnetization m_s ($M \propto m_s \propto (T - T_N)^\beta$) yielding a value of the critical exponent $\beta = 0.325$ ⁸ in agreement with the theoretical 3d-Ising model value³. Diluting the antiferromagnet FeF₂ with non-magnetic ions such as Zn (Fe_xZn_{1-x}F₂) provides a system which in a homogenous magnetic field (Dilute Antiferromagnet in a uniform magnetic field (DAFF)) is a physical realization of the random field Ising model^{9,10}. In Fe_{0.46}Zn_{0.54}F₂, the hysteresis (M-H) curves were found to include an excess moment under field cooled (FC) conditions, somewhat similar to that observed in dilute magnetic alloys such as Ni(Mn), Cu(Mn), Ag(Mn), where a unidirectional anisotropy leads to horizontally shifted hysteresis loops, reminiscent of exchange bias effects¹¹⁻¹⁵. The intercalated transition metal dichalcogenide Fe_xNbS₂ is another compound that shows a peculiar exchange bias (EB) phenomenon, which by Doyle *et al.*¹⁶ was attributed to the coexistence of spin glass and long-range antiferromagnetic ordering.

In this study, we show that an apparent exchange bias observed in the low temperature hysteresis loops of single crystals of FeF₂ originates from a vertical shift of the loops due to an intrinsic excess moment associated with a distortion of the antiferromagnetic structure appearing when passing through T_N in a finite magnetic field.

Results and Discussion

Figure 1 shows the temperature dependence of (a) field cooled (FC); and (b) thermo-remnant magnetization (TRM) curves measured under a constant magnetic field $H = 5\text{ Oe}$ for three different orientations of FeF₂ circular disk; (i) with $H \perp c$ -axis (blue color), (ii) $H \angle 45^\circ$ (green color) and (iii) $H \parallel c$ -axis (red color). The FC and TRM curves exhibit a sharp upturn across the magnetic ordering temperature $T_N \sim 79\text{ K}$, associated with the unbalanced magnetic moment of the two sub-lattices. The T_N determined from the $M(T)$ measurement is consistent with the value of T_N determined from the specific heat data reported by Chirwa *et al.*². The TRM values $\sim 1.1 \times 10^{-3}\text{ emu/g}$ ($1.8 \times 10^{-5}\mu_B/\text{Fe-atom}$) and $0.8 \times 10^{-5}\text{ emu/g}$ ($1.4 \times 10^{-5}\mu_B/\text{Fe-atom}$) at $T = 20\text{ K}$ and $H = 5\text{ Oe}$ for $\perp c$ and

Department of Engineering Sciences, Uppsala University, Box 534, SE-751 21, Uppsala, Sweden. *email: deep.joshi@angstrom.uu.se

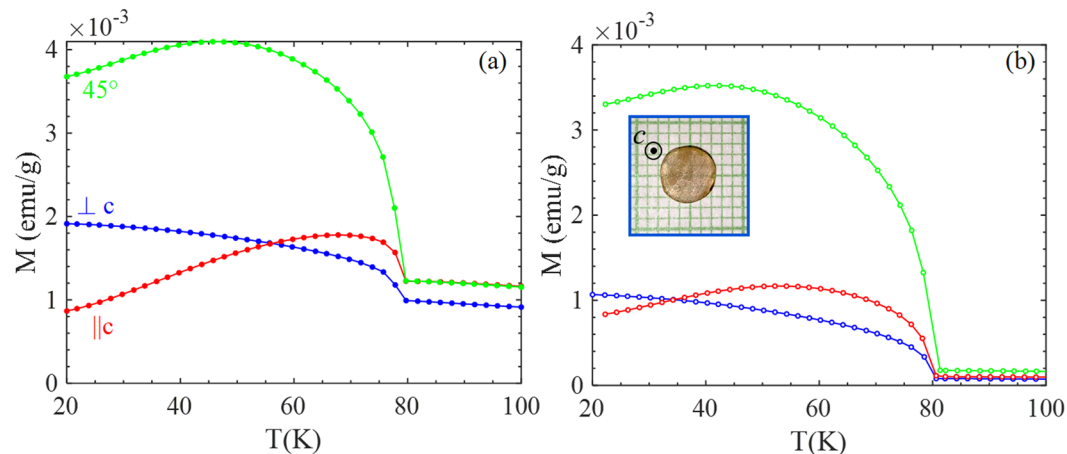


Figure 1. Temperature dependence of (a) magnetization M under FC in a magnetic field of $H = 5$ Oe, and (b) thermo-remnant magnetization (TRM) measured along perpendicular ($\perp c$), 45° and parallel to c -axis ($\parallel c$) of the FeF_2 circular disc. The inset shows a photograph of the top view (along the c -axis) of the FeF_2 single crystal used in experiment.

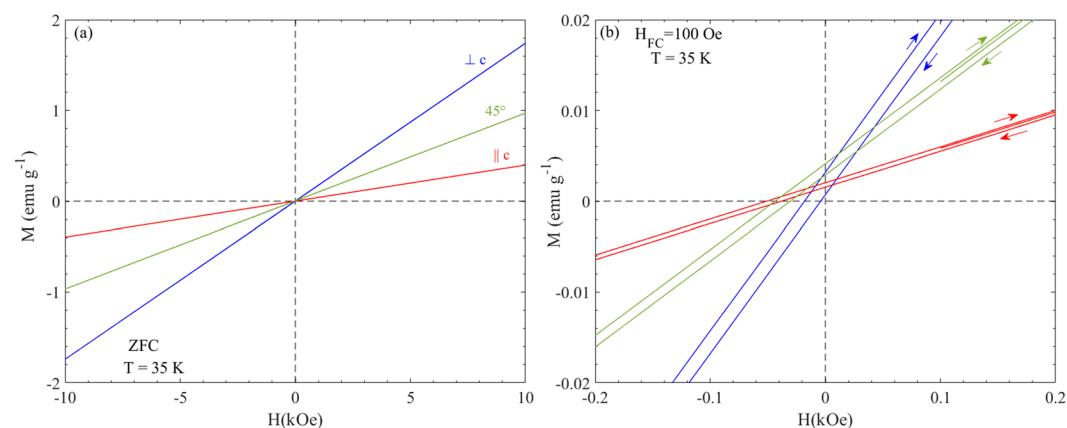


Figure 2. $M(H)$ recorded with (a) field sweep $0 \rightarrow +1 \text{ T} \rightarrow -1 \text{ T} \rightarrow +1 \text{ T}$ after ZFC from 100 K down to 35 K, for three different orientations. (b) $M(H)$ recorded with field sweep $100 \text{ Oe} \rightarrow +1 \text{ T} \rightarrow -1 \text{ T} \rightarrow +1 \text{ T}$ after FC in 100 Oe from 100 K down to 35 K, same color legend as in (a).

$\parallel c$ configuration are also of similar magnitude as earlier reported values of the excess moment^{2,8}; Fig. SM1 in the supplementary material shows the zero field cooled (ZFC) as well as TRM curves in $\mu_B/\text{Fe-atom}$ for reference. Below T_N an irreversibility between the ZFC and FC curves associated with the uncompensated magnetic moments occurs. At higher fields the AFM susceptibility dominates over the FM excess moment and yields a typical AFM $M(T)$ curve for fields parallel to the c -axis, as shown in Supplementary Fig. SM2 for the $\parallel c$ configuration. The combination of AFM susceptibility and excess moment imposes an apparent exchange bias in this system. Figure 2(a) shows the magnetic hysteresis loops ($M(H)$ loops) recorded at $T = 35$ K with field sweep $0 \rightarrow +1 \text{ T} \rightarrow -1 \text{ T} \rightarrow +1 \text{ T}$ after ZFC for $\perp c$ (blue color), 45° (green color) and $\parallel c$ (red color) orientations of FeF_2 single crystal. An apparent exchange bias, shift in the hysteresis loops, is observed for all the three different orientations albeit, as we discussed below this shift is dependent on the cooling and measurement conditions. This shift is more clearly defined when $M(H)$ is recorded after FC with $H_{FC} = 100$ Oe at $T = 35$ K as shown in Fig. 2(b). The observed shift $-H_{EB}$ is 10 Oe, 37 Oe and 40 Oe for $\perp c$, 45° and $\parallel c$ orientations, respectively. This apparent shift in $M(H)$ curves disappear when the curves are recorded at $T = 100$ K ($T > T_N$) as shown in Supplementary Fig. SM3, confirming the coupling between AFM order and FM excess moment below T_N . A shift in the $M(H)$ loops towards opposite direction (right hand side) was noticed when the sample is cooled in a negative field ($-H_{FC}$). The systematic variation of the shift in $M(H)$ curves when cooled in various positive and negative fields ($\pm H_{FC}$) and recorded at $T = 35$ K for three different orientations are shown in Figs. SM4–6. Apart from the apparent exchange bias, there is some irreversibility (horizontal shifts) in the $M(H)$ loops (inset of Fig. 2a). This ‘coercivity’ is an artifact associated with the field-history dependence of the remnant field of the superconducting magnet in the MPMS system¹⁶, which causes a difference between the read off field measure (proportional to the current through the superconducting magnet) and the actual field at the sample. Although, before performing all these measurements we have used the ultra-low field option, a stray/remnant field appears

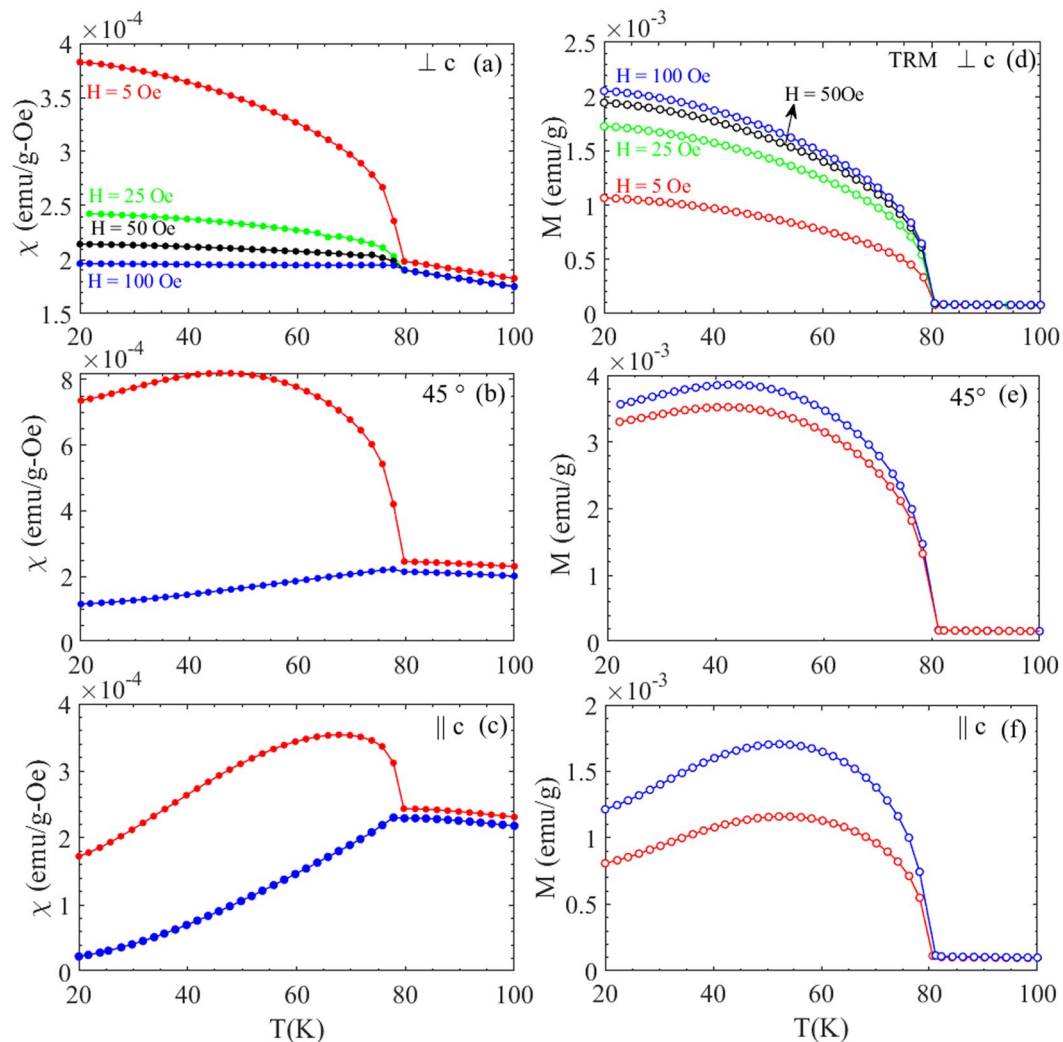


Figure 3. (left) FC magnetization plotted as M/H and (right) the TRM magnetization for two fields ($H = 5$ and 100 Oe) and three different orientation (a) and (d) $\perp c$, (b) and (e) 45° and, (c) and (f) parallel to c -axis ($\parallel c$); in the case of $\parallel c$ configuration data for $H = 25$ and 50 Oe is added. (See Fig. SM1 for SI units and corresponding μ_B/Fe value).

after applying magnetic fields $H > 1$ kOe. As seen in Fig. SM7, the initial value of the magnetization in $M(H)$ measurements recorded after ZFC depends on the weak cooling field remaining in the system. If we limit the maximum field to 1 kOe in $M(H)$ measurements (-1 kOe $\leq H \leq +1$ kOe) the irreversibility vanishes as shown in the inset of Fig. SM7, confirming the artificial origin of coercivity due to stray fields.

Figure 3 displays the temperature dependence of the magnetic susceptibility $\chi(T)$ (left panel) and the TRM (right panel) recorded at two different magnetic fields $H = 5$ Oe and 100 Oe, for $\perp c$, 45° and $\parallel c$ orientations. For $\parallel c$ orientations, data for $H = 25$ Oe and 50 Oe is also added. The representation of $\chi(T)$ in SI units for both ZFC and FC magnetization, and $M_{TRM}(T)$ in μ_B/Fe are shown for reference in Supplementary Fig. SM1. The weak ferromagnetism at low field is attributed to an excess moment locked to the direction of the cooling field. The susceptibility in the $H \angle 45^\circ$ case lies in-between the susceptibilities of $\perp c$ and $\parallel c$ oriented samples as seen from the $M(H)$ curves shown in Fig. 2(a). However, the remnant/spontaneous magnetization for $H \angle 45^\circ$ is nearly three times larger than in the $\parallel c$ case and twice greater than for $H \perp c$, as can be noticed from the $M(H)$ curves in Fig. 2 near $H = 0$ or the TRM curves in Fig. 3e. This behavior may relate to the theoretical observation for some other metal fluorides where the spontaneous piezomagnetic moment has a preferred crystallographic orientation, which is different than the main crystallographic axes^{7,17}.

Figure 4 shows the magnetic hysteresis loops ($M(H)$ loops) after FC in $H_{FC} = 100$ Oe from 100 K down to low temperatures (2 K $\leq T_m \leq 70$ K) for $\parallel c$ orientation. The $M(H)$ data after cooling in $H_{FC} = 25$ Oe and recorded at three different temperatures $T = 50$ K, 35 K and 10 K are shown in Supplementary Fig. SM8 for comparison. As T_m is decreased from 70 K to 2 K, a significant shift in the hysteresis loop towards left hand side as well as decrease in the slope of $M(H)$ curve is observed. To clearly visualize the shift and change in slope (susceptibility), the $M(H)$ curve at $T = 5$ K of the main panel is plotted within the magnetic field range of -0.4 kOe $\leq H \leq +0.4$ kOe in the inset. Here the horizontal and vertical shifts are identified as $-H_{EB}(H_{EB} > 0)$ and M_R respectively; the high field

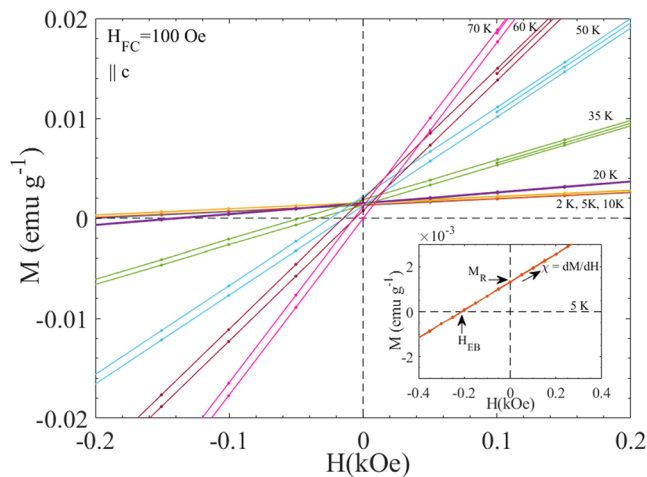


Figure 4. $M(H)$ recorded with field sweep 100 Oe \rightarrow +1 T \rightarrow -1 T \rightarrow +1 T after FC in 100 Oe from 100 K down to low temperature for $\parallel c$ orientation of FeF_2 circular disk. Inset shows the $M(H)$ curve at $T = 5$ K of main panel plotted within the magnetic field range of $-0.4 \text{ kOe} \leq H \leq +0.4 \text{ kOe}$.

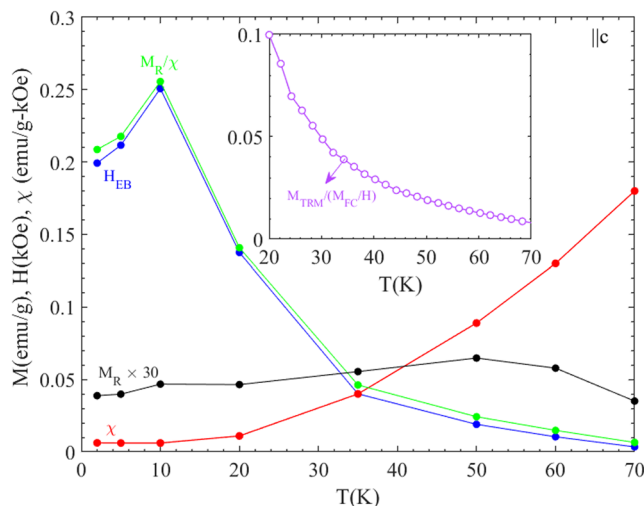


Figure 5. Temperature dependence of H_{EB} (blue color) determined from Fig. 4 for $\parallel c$ orientation. For comparison M_{R} (scaled by a factor of 30 for clear visibility), $\chi = dM/dH$ and M_{R}/χ (green color) extracted from the same $M(H)$ data are also plotted on the same axis. Inset shows the temperature dependence of the ratio of M_{TRM} at 100 Oe (Fig. 3f) and high-field susceptibility M_{FC}/H recorded at $H = 1$ T (Fig. SM2) (in the $\parallel c$ orientation). The close covariation of $-H_{\text{EB}}(T)$ and $M_{\text{R}}/\chi(T)$ demonstrates that the apparent exchange bias observed in FeF_2 stems from its excess moment (M_{R}) and its interplay with the antiferromagnetic susceptibility (χ). As shown in Fig. SM9, the linear shape of the $M(H)$ loops remains even if larger fields (9 T) are applied in the measurements.

slope of the $M(H)$ curve, $dM/dH = \chi$ is also derived. Figure 5 shows the temperature dependence of $-H_{\text{EB}}$, M_{R} (scaled by a factor of 30 for clear visibility), χ and M_{R}/χ extracted from the $M(H)$ data in Fig. 4. The inset shows the temperature dependence of the ratio of M_{TRM} at 100 Oe (Fig. 3f) and high-field susceptibility M_{FC}/H recorded at $H = 1$ T (Fig. SM2) (in the $\parallel c$ orientation). The close covariation of $-H_{\text{EB}}(T)$ and $M_{\text{R}}/\chi(T)$ demonstrates that the apparent exchange bias observed in FeF_2 stems from its excess moment (M_{R}) and its interplay with the antiferromagnetic susceptibility (χ). As shown in Fig. SM9, the linear shape of the $M(H)$ loops remains even if larger fields (9 T) are applied in the measurements.

Conclusion

An intrinsic excess moment is induced in the antiferromagnetic structure of FeF_2 when cooling through the Néel temperature in a finite magnetic field. This moment is confined to the direction of the cooling field and saturates already at cooling fields of order 100 Oe. The magnitude of the excess moment is strongly directional dependent and largest when the cooling field is applied at an angle with respect to the c - and a -axes. The excess moment gives rise to tunable apparent exchange bias due to vertically shifted hysteresis loops. The measured exchange bias becomes large at low temperatures with the applied field along the crystallographic c -axis, since the parallel susceptibility of FeF_2 approaches zero at low temperatures. An apparent coercivity of the high field hysteresis loops measured in MPMS systems (or PPMS systems) is caused by the history dependent remanent field in the

superconducting magnet of the magnetometer. The finding that the excess moment has its largest amplitude at an angle with respect to the main crystallographic axes is consistent with previous results from studies of piezomagnetic effects for some other metal fluorides. Since the works by Dzialoshinskii¹⁷, relatively few theoretical studies have been undertaken to account for these specific effects. There are some studies, which aimed to probe the structure and magnetic properties relationship using pressure in those materials, and we hope that our study stimulates new experimental¹⁸ and theoretical studies⁶ of piezomagnetism.

Methods

The temperature and field dependent magnetization measurements for three different orientations of FeF₂ circular disk (mass 104.56 mg; 5 mm diameter/1.25 mm thick) were performed by using a superconducting quantum interference device (SQUID) magnetometer from Quantum Design Inc (Model:XL) equipped with the ultralow field option. The magnetic field H was applied in the plane of the disk (perpendicular to c axis of the structure, denoted $\perp c$), perpendicular to the plane (parallel to c; denoted $\parallel c$) and with a 45 degree tilt angle with respect to the plane of the disk (45 degree tilted disk, denoted 45°). The dependence of the magnetization M on the temperature T was recorded in zero-field cooled (ZFC) and field cooled (FC) conditions under magnetic fields H of 5 Oe, 25 Oe, 50 Oe and 100 Oe. For ZFC measurement, the sample was cooled to low temperature ($T < T_N$) under zero field, and then the sample was subjected to a constant dc-magnetic field H before recording the data during warming the sample. The FC data was recorded during a subsequent cooling in the same magnetic field. The thermo-remnant magnetization (TRM) was recorded on warming in zero magnetic field, after cooling the sample from 100 K down to 20 K in presence of a constant magnetic field. The field dependence of magnetization M(H) was recorded at a temperature T after zero-field cooling from 100 K down to T_m ; with field swept from $0 \rightarrow +1 \text{ T} \rightarrow -1 \text{ T} \rightarrow +1 \text{ T}$ (ZFC), The M(H) were also recorded under field cooled conditions with field swept from $+H_{FC} \rightarrow +1 \text{ T} \rightarrow -1 \text{ T} \rightarrow +1 \text{ T}$ after field cooling in H_{FC} ($H_{FC} > 0$) from 100 K down to T_m (FC). Measurements with field swept from $0 \rightarrow -1 \text{ T} \rightarrow +1 \text{ T} \rightarrow -1 \text{ T}$ (ZFC) and $-H_{FC} \rightarrow -1 \text{ T} \rightarrow +1 \text{ T} \rightarrow -1 \text{ T}$ after field cooling in $-H_{FC}$ ($-H_{FC} < 0$) from 100 K down to T_m (FC) were also performed for comparison. Before performing all of these measurements, the magnetic field of the magnet was reset to zero by using the ultra-low field option. A Physical property measurement system (PPMS) with VSM option from Quantum Design was used to record M(H) curves up to high fields $H = 9 \text{ T}$.

Received: 16 October 2019; Accepted: 19 November 2019;

Published online: 11 December 2019

References

- Nogués, J., Moran, T. J., Lederman, D., Schuller, I. K. & Rao, K. V. Role of interfacial structure on exchange-biased FeF₂ - Fe. *Phys. Rev. B* **59**, 6984–6993 (1999).
- Chirwa, M., Lundgren, L., Nordblad, P. & Beckman, O. Magnetic specific heat of FeF₂ near T_N . *J. Magn. Magn. Mater.* **15–18**, 457–458 (1980).
- Belanger, D. P. *et al.* Critical behavior in anisotropic antiferromagnets. *J. Magn. Magn. Mater.* **34**, 1095–1096 (1983).
- Le Guillou, J. C. & Zinn-Justin, J. Critical exponents from field theory. *Phys. Rev. B* **21**, 3976–3998 (1980).
- Stout, J. W. & Matarrese, L. M. Magnetic anisotropy of the iron-group fluorides. *Rev. Mod. Phys.* **25**, 338–343 (1953).
- Corrêa, C. A. & Výborný, K. Electronic structure and magnetic anisotropies of antiferromagnetic transition-metal difluorides. *Phys. Rev. B* **97**, 1–8 (2018).
- Borovik-Romanov, A. S. Piezomagnetism in the Antiferromagnetic Fluorides of Cobalt and Manganese. *Sov. Phys. JETP* **38**, 1088–1098 (1960).
- Mattsson, J., Djurberg, C. & Nordblad, P. Determination of the critical exponent β from measurements of a weak spontaneous magnetisation in the 3d Ising antiferromagnet FeF₂. *J. Magn. Magn. Mater.* **136**, 23–28 (1994).
- Belanger, D. P. & Young, A. P. The random field ising model. *J. Magn. Magn. Mater.* **100**, 272–291 (1991).
- Leito, U. A., Kleemann, W. & Ferreira, I. B. Metastability of the uniform magnetization in three-dimensional random-field Ising model systems. I. Fe_{0.7}Mg_{0.3}Cl₂. *Phys. Rev. B* **38**, 4765–4772 (1988).
- Lederman, M., Hammann, J. & Orbach, R. Net spontaneous magnetisation in the dilute ising antiferromagnet Fe_{0.46}Zn_{0.54}F₂. *Phys. B* **165**, 179–180 (1990).
- Hudl, M., Mathieu, R. & Nordblad, P. Tunable exchange bias in dilute magnetic alloys - Chiral spin glasses. *Sci. Rep.* **6**, 2–6 (2016).
- Beck, P. A. Properties of mictomagnets (spinglasses). *Prog. Mater. Sci.* **23**, 1–49 (1980).
- Nogués, J. & Schuller, I. K. Exchange bias. *J. Magn. Magn. Mater.* **192**, 203–232 (1999).
- Ali, M. *et al.* Exchange bias using a spin glass. *Nat. Mater.* **6**, 70–75 (2007).
- Sawicki, M., Stefanowicz, W. & Ney, A. Sensitive SQUID magnetometry for studying nanomagnetism. *Semicond. Sci. Technol.* **26**, 1–16 (2011).
- Dzialoshinskii, I. E. The Magnetic Structure of Fluorides of the Transition Metals. *Sov. J. Exp. Theor. Phys.* **6**, 1120–1122 (1958).
- Ye, Z. *et al.* Pressure-temperature phase diagram and thermoelastic behavior of manganese fluoride up to 13.1 GPa and 700 K. *Mater. Res. Express* **6**, 1–14 (2019).

Acknowledgements

We thank the Stiftelsen Olle Engkvist Byggmästare and the Swedish Research Council (VR) for financially supporting this work. The FeF₂ single crystal was grown (in the late 1970s) by Mr Neil Nighman at University of California Santa Barbara and put to our disposal by Prof. Vincent Jaccarino. Open access funding provided by Uppsala University.

Author contributions

D.C.J., P.N. and R.M. planned and performed the experiments and jointly wrote the final manuscript.

Competing interests

The authors declare no competing interests.

Additional information

Supplementary information is available for this paper at <https://doi.org/10.1038/s41598-019-55142-6>.

Correspondence and requests for materials should be addressed to D.C.J.

Reprints and permissions information is available at www.nature.com/reprints.

Publisher's note Springer Nature remains neutral with regard to jurisdictional claims in published maps and institutional affiliations.



Open Access This article is licensed under a Creative Commons Attribution 4.0 International License, which permits use, sharing, adaptation, distribution and reproduction in any medium or format, as long as you give appropriate credit to the original author(s) and the source, provide a link to the Creative Commons license, and indicate if changes were made. The images or other third party material in this article are included in the article's Creative Commons license, unless indicated otherwise in a credit line to the material. If material is not included in the article's Creative Commons license and your intended use is not permitted by statutory regulation or exceeds the permitted use, you will need to obtain permission directly from the copyright holder. To view a copy of this license, visit <http://creativecommons.org/licenses/by/4.0/>.

© The Author(s) 2019